

Preliminary analysis of deformation at the Eurasia–Pacific–North America plate junction from GPS data

E. I. Gordeev,¹ A. A. Gusev,^{1,2} V. E. Levin,¹ V. F. Bakhtiarov,¹ V. M. Pavlov,¹
V. N. Chebrov¹ and M. Kasahara³

¹Geophysical Service, Russian Academy of Sciences, Petropavlovsk-Kamchatsky, 683006, Russia. E-mail: gord@emsd.iks.ru

²Institute of Volcanic Geology and Geochemistry, Far East Division, Russian Academy of Sciences, Petropavlovsk-Kamchatsky, 683006, Russia

³Institute of Seismology and Volcanology, Hokkaido University, Sapporo, Japan

Accepted 2001 May 23. Received 2001 May 17; in original form 2000 November 6

SUMMARY

Since 1996, a network of nine permanent GPS receivers has been recording, in continuous mode, the deformation on Kamchatka peninsula. The velocity and direction of the relative displacement of observation points are estimated from the entire data set for 1996–2000. The deformation related to the large Kronotskoe earthquake ($M_w=7.8$, 1997 December 5) was identified at distances up to a few hundred kilometres. Half a month before this major event, large-amplitude pre-seismic deformation appeared at stations closest to its epicentral area. The deformation corresponds approximately to a double-couple slow event with $M_w=7.7$ located in the foreshock area, with an orientation that differs significantly from that of the main shock. Clear coseismic displacements were also observed. They match well those predicted by the published Harvard CMT solution. Large-scale post-seismic deformation was also recorded, again with a duration of about half a month, and a cumulative moment comparable to that of the ‘main’ shock. In addition to the transient effects of a large earthquake, data show a secular trend that reflects both the continuous plate motion and the elastic response to interplate coupling. Preliminary estimates of relative plate velocities for the North America, Okhotsk and Beringia plates are given based on the data from stations distant from the most active plate boundaries. Other stations seem to show mainly the elastic response of the Okhotsk and Beringia plates to their coupling with the subducting Pacific plate. At one station at least, the velocity of continuous motion underwent a significant change at the time of the Kronotskoe earthquake, probably indicating a related change in interplate coupling or the effects of mantle rheology.

Key words: arc junction, earthquakes, GPS observation, plate tectonics.

1 INTRODUCTION

Studies of deformation at island arc junctions may clarify a number of still poorly understood problems of contemporary plate motion. On a large scale, a first-order triple junction is present in the Kamchatka area that joins the Pacific (PA), North American (NA) and Eurasia (EU) plates. On a more detailed scale, one should take into account the presence of the smaller Okhotsk (OK) subplate, which can be considered at a larger scale as part of the EU plate. Similarly, Beringia subplate (BE) can be identified as part of the ‘large-scale’ NA plate. Thus, in closer view, there are two conjugate triple junctions: the PA–BE–OK junction located at the abutment of the Kurile–Kamchatka and Aleutian trenches, and the OK–BE–NA junction onland just to the north of the Kamchatka peninsula.

A large proportion of the landmass in this region is favourable for geodetic measurements of surface deformation. The high velocity of PA plate subduction (about 80 mm yr^{-1} ; DeMets *et al.* 1994; Argus & Heflin 1995) produces high-level seismicity and enables one to recover velocities of plate motion even with short-term observations.

During the observation period, the large subduction-type interplate Kronotskoe earthquake occurred near Kamchatka ($M_w=7.8$, 1997 December 5). Its aftershock area is located in the upper part of the continental slope of Kamchatka near the Kronotskii peninsula and spans roughly $220 \times 100 \text{ km}$ along the trend of the island arc (NNE–SSW). Aftershock hypocentres determined by the local network (Gusev *et al.* 1998) define the nodal plane dipping at 23° WNW under Kamchatka as the active fault plane. The earthquake was preceded by a

dense foreshock swarm that began two days prior the main shock, near the NNE end of the aftershock zone. The fault rupture started near this point and propagated about 180 km SSW at a speed of 4.0 km s^{-1} (Gusev & Pavlov 1998). GPS observations revealed well-expressed pre-seismic, coseismic and post-seismic deformation related to this event, as well as high rates of continuous displacement. These observations and their analysis are discussed in this paper.

Recently, the same data set was analysed with respect to coseismic and post-seismic motions by Bürgmann *et al.* (2001). Our analysis was performed before we had access to this paper and is based, in many respects, on different assumptions. In the Discussion section we compare the approaches and results.

2 DATA PROCESSING

The GPS network on Kamchatka has operated since 1996. At present it includes nine sites with continuous measurement of deformation (Fig. 1). At each site, an Ashtech Z12 or Topcon Z12 receiver with a choke-ring Dorne Margolin (ASHDMR) or Geodetic antenna has been installed. The continuous (1 min sampling interval) data flow is accumulated in the memory of a receiver and then extracted daily to a local computer. The entire daily data sets are transmitted through telephone lines to the central computer or recorded to a ZIP disk. All the data are later processed centrally by the GAMIT/GLOBK software, which was developed at the Massachusetts Institute of Technology. As the result of data processing we obtain 24 hr average relative positions of every site with a nominal accuracy of about 3–4 mm for horizontal components that are used in the following. The data set of continuous observations for all stations with respect to PETP is shown in Fig. 2. Note that the

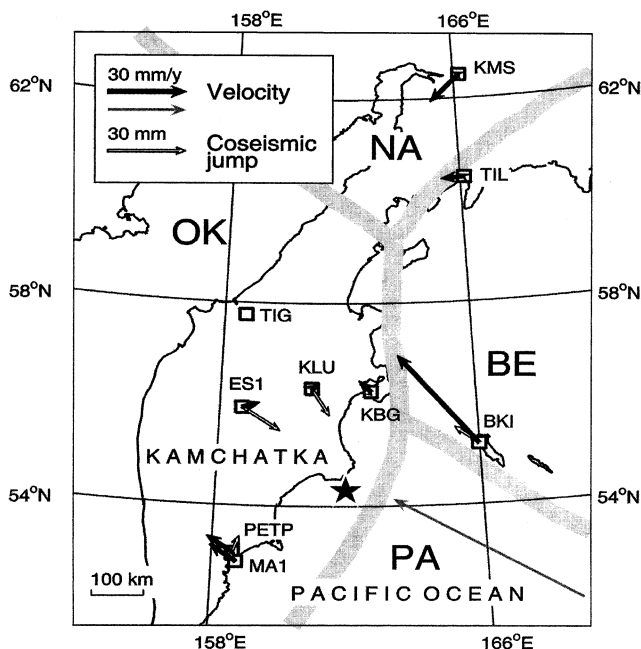


Figure 1. Average velocities of GPS stations (squares) for 1998–2000 and coseismic jumps caused by the major Kronotskoe earthquake of 1997 December 5, $M_w = 7.8$. Station TIG is assumed to be fixed. Grey arrow depicts the velocity of the assumed rigid Pacific plate. Black star indicates the location of the Harvard CMT centroid of the major event. Plates are as follows: PA, Pacific; NA, North American; OK, Okhotsk; BE, Beringia.

reference permanent station PETP is included in the IGS Network as a global station; its data are transmitted daily via the internet to the RDAAS-IRIS global data acquisition centre.

Visual inspection of the data time-series shows many features. Of these, some are technological errors or biases, some evidently represent genuine relative motion of stations, while some cannot be classified reliably or represent a mixture of both. The most easily identified errors are short transients that represent abrupt unipolar excursions of 1–20 day (1–20 reduced data points) duration. However, some short transients are gradual and some look bipolar. Generally, a unipolar transient with a clear return to a slow drifting ‘baseline’ can be reliably discarded as a genuine feature, but this criterion works unequivocally only in a limited number of cases. On the other hand, some properties of the data are evident and correlate between components and/or stations, and they seem to represent genuine relative motion of stations. Unfortunately, the highly erratic (non-Gaussian and highly correlated) style of technological errors prevents the formal detection of earthquake-related transient features. Our identification is informal, and can only be visually verified by the reader.

3 OBSERVED TIME-SERIES

After examination of the entire time-series of 24 hr relative station positions, we considered as genuine the following two classes of features: (1) long-term drift with an approximately constant average rate; and (2) abrupt and gradual step-like or transient features evidently related to the large earthquake ($M_w = 7.8$) of 1997 December 5, which occurred within the GPS network. All these latter features occurred within the ± 1 month period around the large earthquake and include 2(a) coseismic jumps, 2(b) post-seismic signals, seen mostly as a monotonous drift with a decaying rate, and 2(c) pre-seismic signals, appearing as accelerating monotonous drift or a more complicated pattern. Note that many of these features have non-zero total displacement (they are jumps or drift events, not pulse-like) and thus are more likely to be genuine. All numerical estimates for these features are performed at least partly in an informal way because we have no technique at hand to filter out the errors in an automated, statistically grounded way.

Fig. 2 shows the whole time range of reported observations. For data windows in excess of 15 months we consider it possible to estimate the average drift velocity. A prominent feature of the data of station KLU is the clear change in velocity between periods before and after the 1997 December 5 event, suggesting that these two periods should be analysed separately. To simplify the discussion, we will label these two periods as ‘early’ and ‘late’, not to be confused with the 1 month ‘pre-seismic’ period before the event, and the 1 month ‘post-seismic’ period after it. Reliable velocity estimates for the ‘early’ period could be obtained only for KMS and KLU. However, for KMS, a single velocity estimate seems sufficient for both ‘early’ and ‘late’ periods. ‘Late’ velocities could be estimated for TIL, TIG, ES1, KLU, MA1 and BKI (Table 1). Additional estimates of ‘early’ velocities are also given for ES1 and KBG, but these are of low quality because they are derived from single measurements performed about 18 month in advance of the 1997 December 5 event.

Fig. 3 shows relative displacements measured over 65 days prior to and after the large earthquake of 1997 December 5. The horizontal components (N, E) of the six stations BKI,

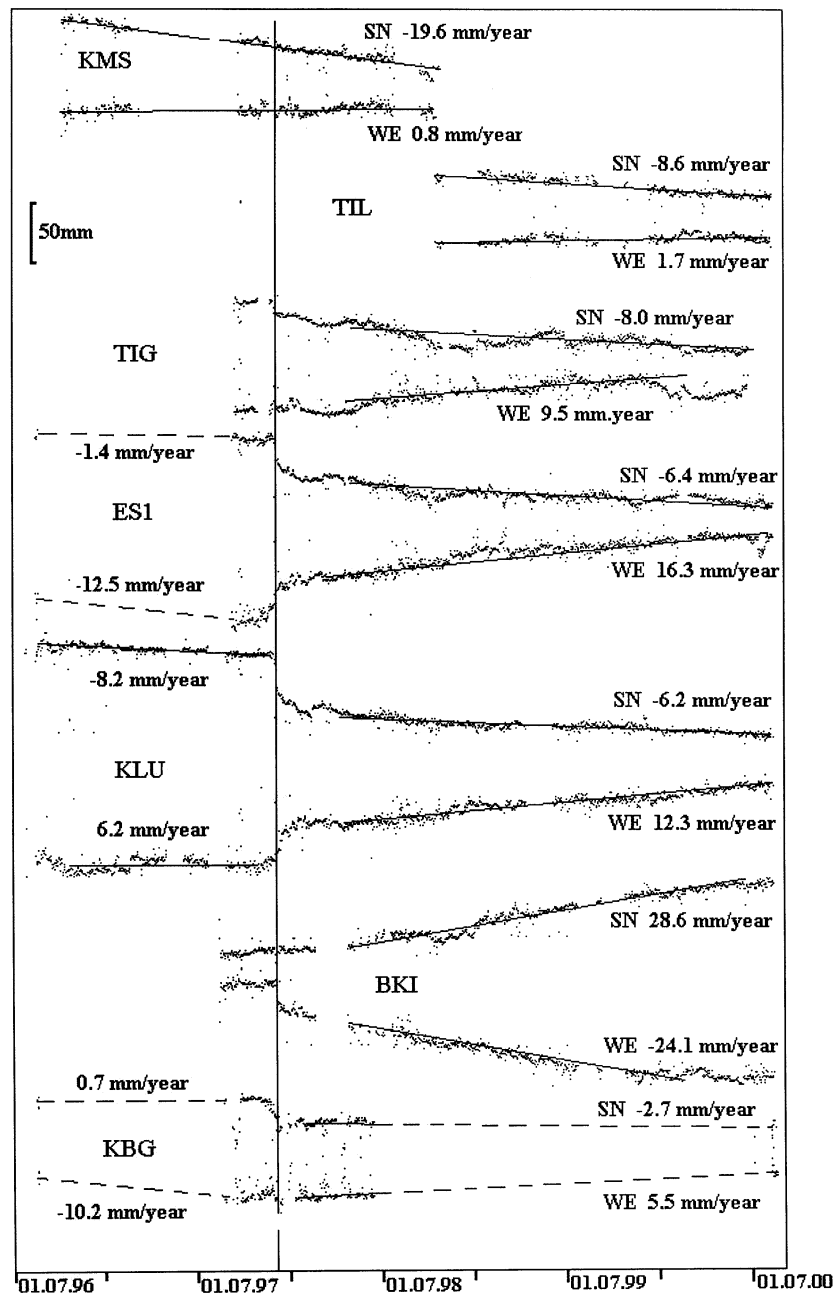


Figure 2. Displacements of seven Kamchatka stations with respect to station PETP along the N and E directions for 1996–2000 and estimates of average velocities. The vertical line depicts the time of occurrence of the $M_w=7.8$ Kronotskoye earthquake of 1997 December 5.

KBG, KLU, ES1, TIG and MA1 are plotted. For TIL and KMS, no data are available close to the time of the large event. The ‘raw’ data points on the plots (circles) are regular 24 hr estimates, each based on a standard unit 24 hr interval, 0 hr to 24 hr UT. A five-point running median filtering is applied to suppress single and double outliers; each result is shown as a solid square plotted at the central (third) point of the five. Note abundant fictitious ‘anomalies’ with duration of 3–10 days or longer that are mostly unaffected by this procedure and thus can be discarded only subjectively. The filtering does not include the 2 days prior to and after the large event. For the 24 hr interval that contains the major event, the ‘raw’ data point is not plotted. The last ‘raw’ data point before and the first point after the large event are marked with diamonds.

Coseismic jumps and drift-like, decaying, mostly monotonous post-seismic signals are evident on most plots. Also, pre-seismic signals can be seen, quite clearly on the traces for KBG-N and ES1-E, less prominently at KBG-E, ES1-N and KLU-E, and somewhat questionably for some other components. To evaluate coseismic jumps, we used two modes. In the first mode (denoted ‘0–24 mode’ in Table 1), the value of the jump was calculated as the difference between two ‘raw’ estimates (diamonds in Fig. 3) adjacent to the 24 hr interval that contains the main $M_w=7.8$ event; data for this latter interval (0 hr to 24 hr UT of 1997 December 5) were discarded. The advantage of this approach is that it employs the standard data processing procedure; however, the discarding of the data adjacent to the causative event is undesirable. To amend this,

Table 1. Velocities of the continuous motion of stations before (1996–1997) and after (1998–2000) the major earthquake of 1997 December 5, and coseismic jumps (CJ) related to this event.

Station, component	Velocity (1996–97) (mm yr ⁻¹)	Velocity (1998–2000) (mm yr ⁻¹)	CJ, 0–24 mode* (mm)	CJ, 12–12 mode* (mm)
BKI, N	–	28.6	+2	–1
BKI, E	–	–24.1	–14	–12
KBG, N	<i>0.7</i>	–2.7	–8?	–8
KBG, E	<i>–10.2</i>	5.5	–6	–6
ES1, N	<i>–1.4</i>	–6.4	–17	–18
ES1, E	<i>–12.5</i>	16.3	+13	+11
KLU, N	–8.2	–6.2	–11	–19
KLU, E	6.2	12.3	+2	+4
TIG, N	–	–8.0	–6	–7
TIG, E	–	9.5	–4	–3
MA1, N	–	–	?	–1
MA1, E	–	–	?	–6
KMS, N	–19.6	–19.6		
KMS, E	0.8	0.8		
TIL, N	–	–8.6		
TIL, E	–	1.7		

The reference station is PETP. Italics indicate low-quality estimates.

*Two modes of evaluation of CJ are described in the text.

an alternative procedure was also used (denoted ‘12–12 mode’ in Table 1), where the value of the jump was calculated as the difference between the estimates for two immediately adjacent non-standard, shifted 24 hr intervals, 12 hr to 12 hr UT. In this mode, the origin time of the main event (11 hr 23 min UT) almost coincides with the boundary between new intervals (12 hr 00 min UT). To calculate estimates in this case, the extrapolation of daily satellite orbit ephemerides by 12 hr was employed within the processing procedure. The two approaches gave quite comparable results (see Table 1). The results of the second procedure were taken as the final estimates for coseismic jump.

To quantify pre-seismic and post-seismic signals, the following approach was taken. First, we visually inspected the data and found that for a number of discernible pre-seismic features (KBG-N, KBG-E, ES1-N, ES1-E KLU-N and KLU-E), a common duration of 15–20 days can be chosen. It should be noted that pre-seismic signals do not have a definite shape: at

KBG-N, ES1-E and KLU-E, the signal behaves more or less like a monotonous, accelerating drift, whereas at KBG-E and ES1-N, the signal is rather like a pulse (‘bay-like’). At KLU-N, the shape is complicated, seemingly with a change in sign at day –5. A low-amplitude pulse-like signal of 15–20 days duration is also suspected at BKI-N, but we did not include this highly doubtful case in our analysis. The special case is TIG-N, where an accelerating monotonous pre-seismic feature seems to be present, but with smaller duration, of about 7 days. The data for TIG-E we rated as generally unreliable, with a number of fictitious anomalies; we use only the coseismic and total jump estimates for this trace. Note that different pre-seismic signal shapes on different components suggest that there is no single source for this signal; this point will be discussed later.

Although the presence of post-seismic signals is obvious, the choice of visual durations for them is not unambiguous. There are two distinct alternatives for KLU and ES1, of about 10–20 or about 35–50 days. For KBG, TIG and MA1, however, durations seem to be less than 20 days. The case of BKI is intermediate. It should be mentioned that for many components, one more selection for the duration of post-seismic signal is possible, of around 3–4 months. This possibility is readily seen in Fig. 2, where the size of the gap between the major event and the left end of the linear segment that represents the continuous drift defines, approximately, the value of the duration. In the present preliminary study we decided, somewhat arbitrarily, to select systematically the shorter variant of duration, less than 20 days. We have already noted that the shape of most post-seismic signals is, approximately, a decaying drift; the special case is MA1, where the post-seismic feature is instead pulse-like.

After visually selecting post-seismic signal duration for each station, we determined ‘zero lines’ for pre-seismic and post-seismic signals. To obtain these, 10–20 day reference time intervals were chosen on each plot, before and after the assumed signal. Within these intervals, medians over data points were determined and then employed as reference levels. These time intervals and levels are shown as thick grey bars in Fig. 3; thinner grey lines are the extrapolations towards the date of the major event. The values of the total displacement jump are obtained as the differences of these reference levels (see Table 2 for these and other signal parameters). Also, the values of amplitude for each pre-seismic and post-seismic signal were determined with respect to the same levels.

Table 2. Parameters of pre-seismic (PRS) and post-seismic (POS) signals, and values of the total displacement jump (TJ).

Station, component	PRS duration (days)	PRS amplitude (mm)	Sign match to CJ*	POS duration (days)	POS amplitude (mm)	Sign match to CJ*	TJ (mm)
BKI, N	20??	0	na	na	0	na	–2
BKI, E	na	0	na	14	–9	+	–23
KBG, N	17	–10	+	12	–12	+	–22
KBG, E	14	+3	–	10–15	–5	+	–9
ES1, N	18	+3	–	17	–13	+	–26
ES1, E	18	+16	+	16	+5	+	+27
KLU, N	17	+3	–	17	–18	+	–41
KLU, E	18	+3	+	17	+19	+	+27
TIG, N	7	–5	+	16	–4	+	–13
TIG, E	na	na	na	na	na	na	+3
MA1, N	na	0	na	16	–3	+	–4
MA1, E	na	0	na	18	–3	+	–2

The reference station is PETP. na: not available.

*The sign of the PRS/POS coincides with (+) or is opposite to (–) the sign of the coseismic jump.

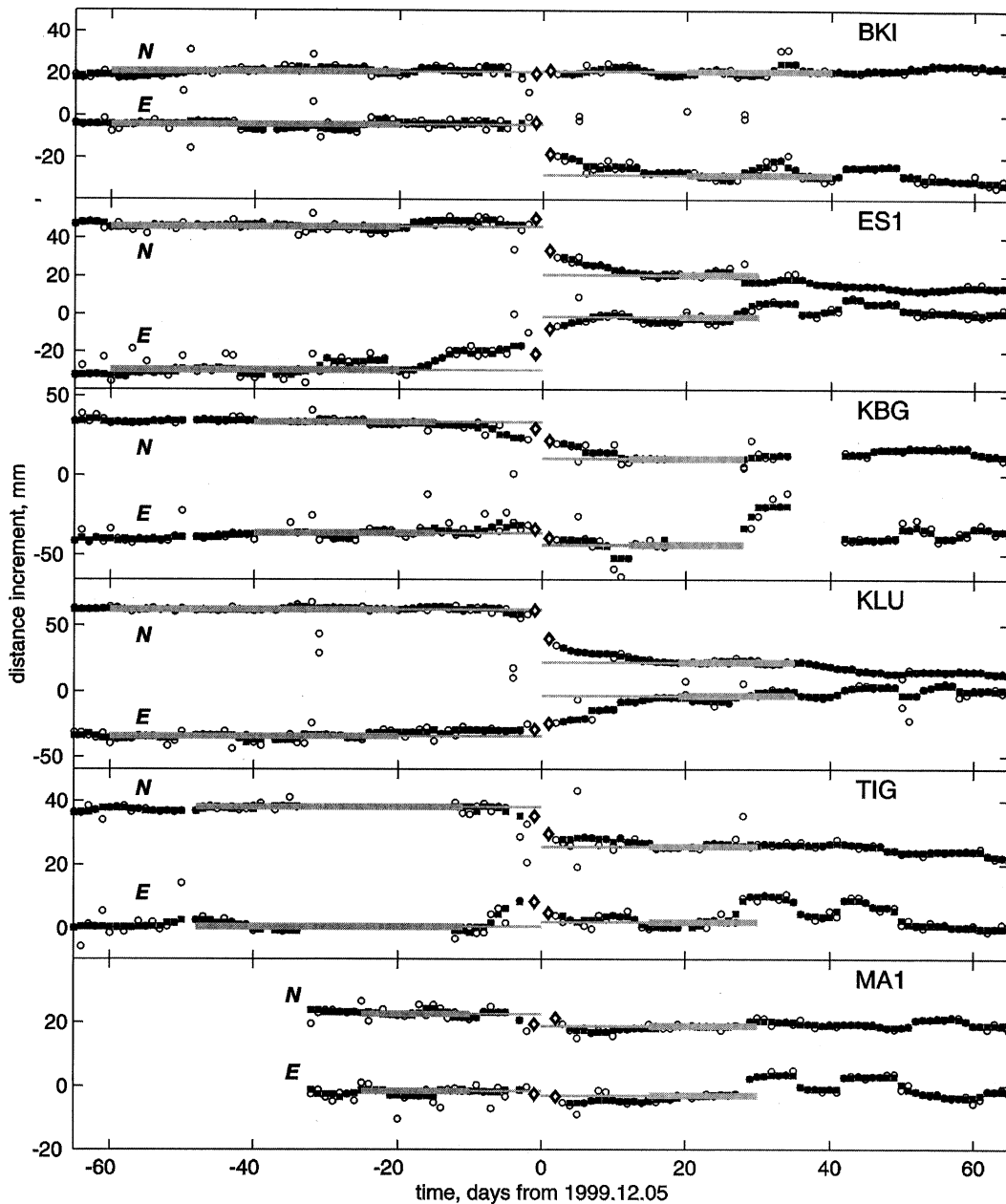


Figure 3. Displacements of six Kamchatka stations with respect to station PETP along N and E directions during the time interval ± 65 days around the major earthquake of 1997 December 5. Circles: raw 24 hr data; squares: their running five-point medians; diamonds: 24 hr estimates for 1997 December 4 and 1997 December 6; the difference in their levels defines the coseismic jump; grey bars: pre- and post-event reference levels, assumed stable, each defined by the median over the data points covered by a bar; grey lines extrapolate these levels towards the date of the major event. Clear post-seismic and reasonably well defined pre-seismic variations are seen on many components.

In Table 2, we show the results of comparing the signs of pre-seismic and post-seismic signals with those of coseismic jumps: there is an excellent match for post-seismic signals, whereas for pre-seismic signals, no correlation is seen.

4 ANALYSIS OF OBSERVATIONS

4.1 Average velocities

In the following we analyse the average velocities given in Table 1, with PETP as the fixed point. As already noted, regular

estimates of continuous velocity for the 'early' period (before 1997 December 5) could be obtained for KLU and KMS only; for the 'late' period (after 1997 December 5), velocities of seven stations could be determined. For KMS, neither a coseismic jump nor a change in velocity in December 1997 is seen; we thus calculated a single common velocity estimate over the entire time span 1996–2000. For KLU, a clear difference in velocity is present between the 'early' and 'late' periods. Unfortunately, with regular data from only two stations for the 'early' period, no meaningful constraints on plate motions can be derived for this period. There are, additionally, low-quality estimates

for two more stations, but using these data does not produce any consistent picture. For this reason, we further analyse the velocities for the 'late' period 1998–2000. To make this analysis visually clearer, the use of PETP as the reference station is not desirable. On a day-by-day basis, using this station as the standard reference was the only reasonable choice, because the record for this station is the most complete and its maintenance most reliable. However, to represent the average relative plate motion visually, we prefer the use of a fixed station that is not so near to the plate edge. For this reason, the relative velocity vectors were recalculated with TIG taken as the new reference point, and are plotted in Fig. 1. When one compares the observed picture with the known plate structure around Kamchatka, one comes to the following preliminary conclusions.

(1) The KMS versus TIG velocity can be related to the motion of the NA plate versus that of the OK plate; the type of motion is nearly pure SW–NE compression at a velocity of about 1.8 cm yr^{-1} . Station TIL is very near to the NA–BE boundary and the rigid plate motion estimates based on its data may be biased. We nevertheless note that, formally, using TIL as a reference for the BE plate, we find from the TIG–TIL pair that BE versus OK motion is approximately E–W pure compression at about 0.7 cm yr^{-1} . From the TIL–KMS relative motion we similarly obtain NA–BE motion as oblique N–S compression at a rate of about 1.2 cm yr^{-1} .

(2) The BKI versus TIL vector (which is only slightly different from the BKI versus TIG vector of Fig. 1) represents mainly the elastic deformation of the BE plate at its BE–PA boundary, which is very close to BKI. An ideal reference position for detecting such deformation would be far within the BE plate. The actual position of TIL is near the BE–NA boundary. However, the BE–NA boundary is a secondary one, with limited seismic activity, and can be tentatively ignored in a first approximation. After such a simplification we note that the observed velocity vector agrees reasonably well with that expected from the elastic response of the BE plate to its coupling with the PA plate, that is, shear-style WNW drag of the plate edge with a velocity (5 cm yr^{-1}) near to half the relative rigid plate velocity of about 8 cm yr^{-1} .

(3) Similarly, almost parallel motion of PETP, MA1 and KBG with respect to TIG qualitatively agree with the motion expected from the elastic response of the OK plate to its coupling with the subducted PA plate, that is, compression-style WNW drag of the plate edge. Relative motions of KLU and ES1 with respect to TIG are smaller and not systematic; this generally agrees with the much smaller motions expected here on the basis of coupling.

(4) There is a significant change in velocity at station KLU between the 'early' and 'late' periods of observation. This change is determined fairly reliably. Significant changes may also exist at ES1, BKI and KBG, but these are much less reliable because of the low data quality for the 'early' period. On the other hand, no such change exists for station KMS. Note that all of these changes are determined relative to PETP. The changes seem to be related to the large earthquake of 1997 December 5. Tentatively they may be associated with the coseismic change of coupling of PA versus OK and PA versus BE. Another possible explanation is the difference between plate-edge deformation rates for the cases of almost relaxed asthenosphere (before the large earthquake) and of effectively elastic asthenosphere (just after the earthquake).

4.2 Pre-seismic signal

We now proceed to the analysis of shorter-term variations. In this case, we return to the use of PETP as the fixed reference. (Stations that are further from the plate boundary such as TIG or KMS would be more advantageous fixed points; however, the use of TIG is undesirable because of probable technological errors on one of the components, and the use of KMS is impossible because of the data gap).

As already noted, pre-seismic signals do not show any definitive, common time function either on two horizontal components of the same station or at different stations. This may indicate that the pre-seismic signal is not produced by a single moment tensor source. Rather, the source may consist of several point sources with various time functions. Unfortunately, the limitations of data volume make the multiple-source possibility difficult to analyse, and such an analysis is left for the future. Our preliminary study is based on the aforementioned possibility of choosing pre-seismic signal anomalies with comparable durations of about 15 days and comparable monotonous or pulse-like shapes on a few channels. This fact suggests that the entire set of pre-seismic signal features can be treated as a manifestation of a single deformation event. If this tentative approach fails, this would show that a single-source assumption is completely incorrect. If it does not fail, we will have some evidence that the precursory deformation process was mechanically organized and not completely erratic. We selected the amplitudes of the pre-seismic signal both for monotonous features and for pulse-like features with similar duration (Table 2, Fig. 4). For TIG–N we use the amplitude of the monotonous pre-seismic signal with a 7 day duration. Although most stations with large pre-seismic signal amplitudes also exhibit large coseismic jump amplitudes (Fig. 5), the orientation of pre-seismic signal and coseismic jump vectors is rather different. We assume, further, that displacements are caused by a 'slow earthquake' of about 15 days duration located at the centre of the foreshock swarm, at the NNE edge of the source of the main shock. We inverted the amplitude data, treating them as static displacements resulting from a deviatoric moment tensor point source embedded in an elastic half-space ($\mu = 5.7 \times 10^{10} \text{ N m}^{-2}$). In the inversion procedure, no data weighting was applied because we believe that the errors in the estimates of displacement are comparable for all components and stations. Low-accuracy data on vertical displacements were discarded. To characterize the misfit we use the value of rms residual (observed minus computed) of displacement components, normalized by the rms observed displacement; this is denoted 'relative error' (RE).

The resulting source has a moment magnitude $M_w = 7.7$, and its double-couple parameters are given in Table 3 and shown in Fig. 4. The recovered moment tensor is very near to a double-couple. Its orientation does not significantly contradict the dominating stress regime of the convergent OK–PA plate boundary (that is, WNW–ESE horizontal contraction). For the calculated and observed directions of displacement vectors, the fit is acceptable, but the misfit between displacement amplitudes is considerable, in particular for ES1. The general fit is marginal to poor, expressed by a relative error of 0.75.

We also tried to fit the same data assuming a general (deviatoric + volumetric) seismic moment tensor. In this case the least-squares solution was unfortunately unstable, indicating that the data set is too poor to resolve a volumetric component

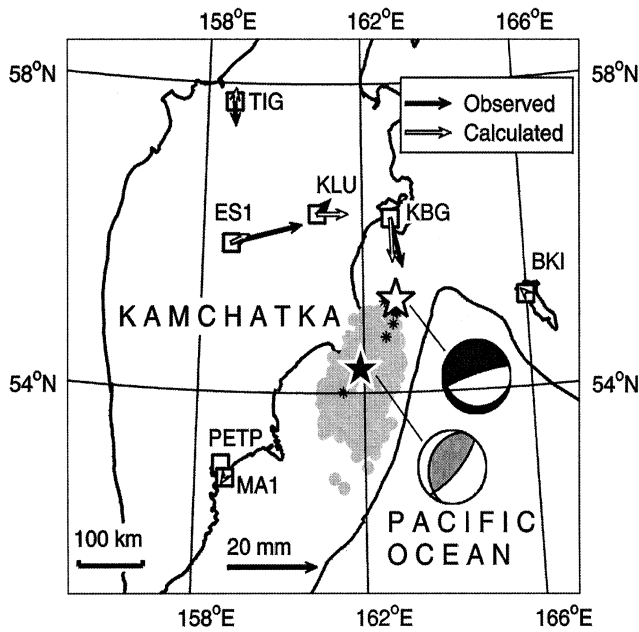


Figure 4. Pre-seismic motions before Kronotskoye earthquake with respect to PETP, and the result of their fit by inversion for a deviatoric moment tensor point source (shown as the black and white beachball). The assumed location of the model source (white star) is within the foreshock area, at a depth of 30 km. Foreshock epicentres are denoted by asterisks. Although the orientation of displacement vectors is predicted well, the general fit is far from satisfactory. The fitted source is equivalent to an $M_w=7.7$ event. The black star and grey and white beachball denote the best double-couple for the Harvard CMT solution of the main shock. Grey dots are the epicentres of the first-day aftershocks. Both the observed and the expected static motion at KBG are *towards* the source, whereas the expected P -wave motion for our inverted solution is *away from* the source.

of the moment tensor. However, without any inversion one may note that the orientation of the displacement vectors speaks against the presence of a dominant explosion/implosion component. Indeed, in such a case, displacement vectors should all point either away or towards the epicentre, whereas in reality they mostly point in a tangential direction. Thus, the dilatancy zone hypothesis is not supported by the data. In a number of other tests, we assumed that a single deviatoric source is situated in a number of trial locations near station

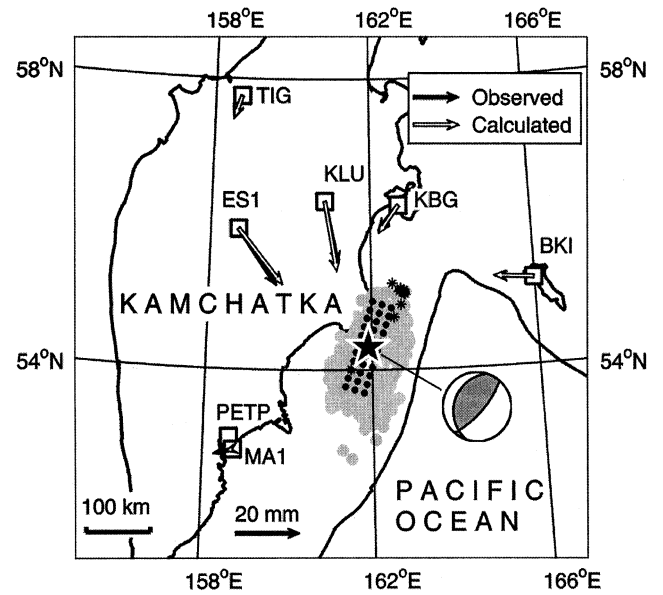


Figure 5. Observed coseismic displacement jumps caused by the Kronotskoye earthquake and calculated for the point source specified by the Harvard CMT solution. The reference station is PETP. The observed and calculated jumps at stations BKI, KBG and TIG are practically identical. Jumps were also calculated for the extended model source (black dots), located within the 'subduction' nodal plane, with the same moment tensor as the Harvard CMT solution. Jump vectors for the extended source are not shown because they practically coincide with those obtained for the point source. For other notation see the caption to Fig. 4.

ES1, where the largest displacement is observed, and not in the main Benioff zone. The resulting solutions, however, did not show any improvement; rather, they spoiled the general fit. To conclude, we believe that we have obtained a very rough approximation of the scale and orientation parameters of the source of the pre-seismic signals. However, important details of these signals are still unexplained.

We reiterate that the present data do not permit us to *prove* the presence of precursory deformation. First, the identification was informal. Second, in the selection of pre-seismic signals (as well as of post-seismic and coseismic signals) we implicitly but very extensively used the fact that the main shock date was known *a priori*. Over the entire observation period, excursions

Table 3. Best double-couples of seismic moment tensors.

Tensor*	ϕ (°N)	λ (°E)	h (km)	M_0 (10^{20} N m)	M_w	nodal plane 1		nodal plane 2		NDC† (%)	RE‡ (%)
						strike (°)	dip (°)	strike (°)	dip (°)		
PRS, inv.	55.2	162.8	30	4.2 ± 3.4	7.7	252	79	100	12	5	75
CJ, HDC	54.3	161.9	33.6	5.3	7.8	202	23	39	68	5	15
CJ, HDCe	54.3	161.9	23, 33, 43	5.3	7.8	202	23			5	20
CJ, inv.	54.3	161.9	33.6	6.2 ± 1.7	7.8	198	21	39	70	1	13
POS, inv.	54.0	162.0	30	7.6 ± 9.9	7.9	210	21	80	76	15	44
TJ, inv.	54.3	161.9	30	11.4 ± 3	8.0	196	39	63	62	18	19

* Abbreviations denote inversions of pre-seismic (PRS) and post-seismic (POS) signals, coseismic (CJ) and total displacement (TJ) jumps; 'inv.' is our solution for a deviatoric point source obtained by inversion of GPS data; 'HDC' is the best double-couple that corresponds to the Harvard CMT solution; 'HDCe' denotes the extended source with total moment equal to that of the 'HDC' case.

† Non-double-couple component.

‡ Relative rms residual error.

of comparable size can be found, and some of them are even correlated between data channels. We treat some of them as technological biases; others may represent a genuine Earth signal. However, they never show so visually consistent a picture as that in Fig. 3.

4.3 Coseismic jump

The coseismic displacement vectors (Table 1), with PETP taken as the reference station, are plotted in Fig. 5, together with theoretical displacement vectors that were calculated for a point source embedded in an elastic half-space ($\mu = 5.7 \times 10^{10} \text{ N m}^{-2}$). The point source was specified according to the best double-couple of the Harvard CMT solution for the 1997 December 5 event (Dziewonski *et al.* 1998). The match is completely acceptable. The full CMT solution (Table 3), with a 5 per cent non-double-couple component, produces displacement vectors that are visually indistinguishable. In addition to the point source model, an extended source mode was studied, modelled by a $150 \times 50 \text{ km}$ array of identical point sources (11×3 points) with the same total tensor, located approximately along an assumed 'subduction' nodal plane (No 1 in Table 3) of the 1997 December 5 event, dipping under Kamchatka. This nodal plane can be selected quite reliably on the basis of aftershock hypocentres determined by the local network (Gusev *et al.* 1998). For this source, the match of predicted and observed displacements is comparable to that of the point source. For completeness, we also give in Table 3 the result of the inversion of coseismic jump data, which is almost identical to the Harvard CMT solution.

4.4 Post-seismic signal

The identification of post-seismic signals in the observations (Fig. 3) is more reliable than that of pre-seismic signals; it is partly simplified by the good correlation of the signs of the coseismic jump and the post-seismic signal (see Table 2). The amplitudes of post-seismic displacement vectors are shown in Fig. 6 and listed in Table 2. We assume that displacements followed a common post-seismic time function whose shape is, approximately, an exponential monotonously decaying drift that becomes unobservable about 18 days after the event. The time constant for the exponential decay is of the order of 6 days. The source of this anomaly is modelled by a deviatoric moment tensor point source that cannot be very different in position and orientation from the centroid of the main event. Note that the stations with large post-seismic amplitudes also recorded large coseismic jump amplitudes, and the orientation of post-seismic signals and coseismic jump displacement vectors is fairly close. To make an interpretation of these data, we assume that the coseismic slip was followed by a slow event with comparable orientation and a duration of about 18 days. As for the location of the slow earthquake, a number of possibilities were analysed. The first possibility is based on the idea that the post-seismic slip was the immediate continuation of the slip of the main event and took place over the *same fault area*. For this case, we locate the point source at the approximate centre of the aftershock swarm of the 1997 December 5 event, at a depth of 30 km. The recovered double-couple source has a moment magnitude $M_w = 7.9$, and its orientation is given in Table 3 and plotted in Fig. 6. Within large error bounds, its estimated

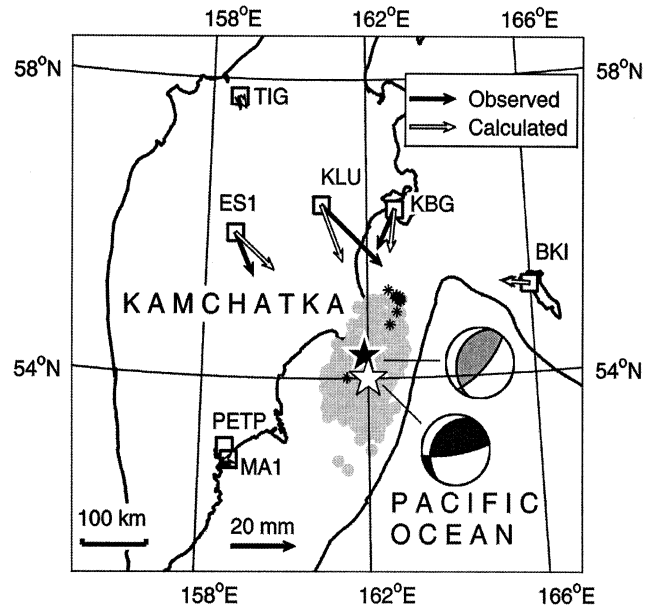


Figure 6. Post-seismic motions after the Kronotskoye earthquake and their fit from their inversion for a deviatoric moment tensor point source. The assumed location of the model source is within the aftershock area at a depth of 30 km (white star); its focal mechanism is shown by the black and white beachball. The source is equivalent to an $M_w = 7.9$ event. The observed and calculated vectors at station BKI are practically identical. For other notation see the caption to Fig. 4.

scalar seismic moment is similar to that of the 'fast event'. The post-seismic signal moment tensor solution is close to that of the main shock, and the fit of the calculated displacement vectors to the observed ones is quite acceptable. Another possibility is that the aseismic slip took place *beyond the fault area* of the fast-event source, but still on the interplate boundary. We considered two variants, putting the point source in either the downdip or the updip continuation of the fault plane of the 1997 December 5 earthquake at depths of 75 and 15 km, respectively. In both cases, the fits of observed and theoretical displacements were definitely worse than in the first case, thus making the idea of propagation of slip along the interplate boundary improbable.

4.5 Total jump

Because of the similarity of the 'fast-earthquake' and 'post-seismic' dislocation mechanisms, the double-couple mechanism inferred from the moment tensor inversion for the total displacement jump is similar to both the coseismic jump and the post-seismic signal solutions (Table 3). The seismic moment related to the entire sequence of events from 1997 November 15 to 1997 December 25 is equivalent to $M_w = 8$. It must be noted that the sum of scalar seismic moments of the pre-seismic, coseismic and post-seismic events is not identical to the value found from the total jump. This difference is due to the combined effect of the following factors: the low accuracy of scalar seismic moment estimates, differences among orientations of best double-couples, and differences among point source locations. Despite this problem, we made a very rough estimate for relative contributions of the three 'components' to the total

seismic moment. The main contribution (some 45–50 per cent) is from the post-seismic motion, the coseismic motion contributes 35–40 per cent, and the pre-seismic motion contributes the rest.

5 DISCUSSION AND CONCLUSIONS

The mostly continuous measurements from 1996 to 2000 of surface deformation by GPS instruments at nine sites on the Kamchatka Peninsula revealed movements between the PA, NA and EU plates. The continuous displacement rates of the GPS stations relative to TIG (Fig. 1), which is located relatively deep on the OK subplate of the EU plate, reveal the relative motions of the NA, OK and BE plates (Fig. 1). However, even for stations not located near the most active (PA–OK and PA–BE) boundaries, the estimated motions for 1998–2000 cannot be treated as true long-term velocities, because lower-quality data for 1996–1997 suggest that velocities during these two periods were different. In one case, for station KLU, this difference is relatively well established. This change may indicate a change in the level of coupling related to the 1997 December 5 earthquake. The velocity seems to be smaller before than after the earthquake, in agreement with the cyclic model of stress and displacement rate in a strongly coupled subduction zone (Taylor *et al.* 1996). The displacement rates outside the subduction zone on the border between the NA and OK plates seem to be unaffected by the large earthquake, and to stay at a constant value (Fig. 2, station KMS). Note that the kinematic picture presented is very preliminary. Relative motions of pairs of assumed rigid plates are deduced from the motions of single station pairs and cannot be verified independently; also, for the BE plate, both available stations (TIL and BKI) are near to its boundary. Motions at BKI, KBG, PETP and MA1 seem to agree qualitatively with those expected for an elastic response related to plate coupling.

Recently, Takahashi *et al.* (1999) discussed the GPS data for motions on and around the Okhotsk plate. They used the station set that included two of the nine stations analysed here (PETP and KLU). Their estimates of continuous velocities are all for our ‘early’ period (before the 1997 December 5 event); they do not contradict our conclusions.

As was shown previously (Taylor *et al.* 1996; Klotz *et al.* 1999), the rate of plate convergence related to large earthquakes probably controls the stress regime in and near a coupled subduction zone. The oceanic plate, descending slab and continental lithosphere respond elastically to temporal variations of stress and displacement rate related to the earthquake cycle. The contradiction between the high deformation rate in the Aleutian–Alaska subduction zone near Kodjak island (Savage *et al.* 1999) and negligible deformation in the Shumagin islands (Lisowski *et al.* 1988; Larson & Lisowski 1994) was explained as a high strain rate at the beginning of the earthquake cycle (Alaska Earthquake, 1964) and a low strain rate in the middle or late part of the cycle (Shumagin gap). In our case, we have data for displacement rates at a particular section of an island arc, and they show, in a similar manner, a significant change between the end of one interseismic period and the beginning of another.

The identification of preseismic motion deserves discussion. When looked at on a station-by-station basis, the pre-seismic motions are well detected and seem to represent a genuine

phenomenon. First, they are seen on a number of stations and components. Second, the time functions of the signal for different stations and components, although far from being completely identical, have a comparable duration and a simple (unipolar or pulse-like) shape. Third, their amplitude is relatively large. On the other hand, when these data are analysed jointly, we find the relatively poor fit of pre-seismic signal data by a single deviatoric point source and the lack of a truly common shape for time functions. These facts suggest that the precursory process was rather complicated, and included several components, probably with various locations and time functions. The success, although limited, of inversion of the pre-seismic signal in terms of deviatoric source indicates that this type of source is permissible. On the other hand, the data do not support a source model with a dominant explosion/implosion source component, for example, like one that follows from the precursory dilatancy hypothesis. As for the size of the source, although its preliminary characterization by $M_w=7.7$ may be revised in future studies, it is unlikely that its scalar moment will be reduced by more than a factor of three. To conclude, we were fortunate to observe and (post factum) to identify a genuine medium-to-short-term deformational precursor of a large earthquake.

Post-seismic motions are, generally, much less unusual. They fit well the idea of slow, creep-style continuation of slip over the same ‘fast-earthquake’ fault area, with a similar direction of slip. Preliminary checks are against the idea of the propagation of the slipping patch of the interplate interface far outside the ‘fast’ fault area, either downdip or updip.

Recently, Bürgmann *et al.* (2001) analysed the same data with an emphasis on the properties of the post-seismic slip. In our work, we were not aware of this study. It is interesting and instructive to compare the results of independent studies based on somewhat different assumptions. First, when analysing possible pre-seismic displacements, Bürgmann *et al.* (2001) consider only the time span of the foreshock sequence (the last 49 hr before the main shock) and find no evidence of pre-seismic motions within this period. Indeed, so short a segment of data does not show any clear evidence of pre-seismic variations; even for the much longer sequence analysed by us, the detection of the pre-seismic signal was made in an informal way only. Second, they fit the data, both for coseismic and post-seismic displacements, by an extended fault model only, with some parameters constrained. From two to six parameters out of seven—length, width, strike, dip, rake and centre coordinates—were constrained in various inversions. This is rather different from our approach, in which we looked for a point source with a fixed location and general deviatoric seismic moment tensor. Most indicative in this situation is to compare scalar seismic moment estimates. Both groups found that the seismic moments related to the main shock and to the post-seismic slip are comparable. The absolute estimates of Bürgmann *et al.* (2001) are about 70 per cent of ours, in approximate agreement with the difference of the assumed value of shear modulus ($3.0 \times 10^{10} \text{ N m}^{-2}$ against our $5.7 \times 10^{10} \text{ N m}^{-2}$). Our selection for the duration of the post-seismic slip accumulation differs significantly: 15–20 days in our case against 50–55 days for Bürgmann *et al.* (2001). We have already mentioned that a duration of about 3–4 months for the post-seismic signal is also a possible choice. This third choice is based on the time when the post-seismic drift finally stabilizes and acquires, very approximately, a constant velocity (related to continuous, secular

motion). This point evidently deserves a more detailed study. One more difference regards the location of the post-seismic slip event. Our tests, although very limited, did not indicate the propagation of slip far beyond the main shock fault area. Using the results of one (constrained) inversion, Bürgmann *et al.* (2001) propose a certain downdip shift of the post-seismic slip area, based on the fact that the estimated centroid depth shifts to 41 km, as compared to the constrained 30 km depth, assumed true both for the main shock and for the afterslip. However, their unconstrained depth estimate for the main shock was 58 km, and this fact could be used to derive the opposite conclusion. In our opinion, the data quality does not permit one to resolve reliably such fine details. One remarkable conclusion of Bürgmann *et al.* (2001) is that post-seismic slip was a complicated process that is difficult to fit by a single dislocation plane. This fact agrees with our relative error value for the post-seismic event (44 per cent) as compared with that for the main shock (13 per cent). In general, the results of the two groups are quite comparable.

The coseismic deformation related to the large subduction earthquake ($M_w=7.8$) is in excellent agreement with that calculated from the dislocation model based on the published Harvard CMT solution. This fact is very important: it confirms the reliability of the entire measurement system and specifically the good quality of short-term GPS data. At the same time, it means that the Harvard CMT solution is a reliable estimate of true seismic moment tensor of the source.

ACKNOWLEDGMENTS

This research was partly supported by the Ministry of Science and Technology of the Russian Federation. We would like to thank R. King from MIT for providing the GAMIT software, which was used for data processing. Constructive comments by Associate Editor Günter Bock and two anonymous referees have significantly improved the paper. We are grateful to the personnel of the seismic stations of KEMSD, who helped to provide the continuous GPS data collection.

REFERENCES

- Argus, D.F. & Heflin, M.B., 1995. Plate motion and crustal deformation estimated with geodetic data from the Global Positioning System, *Geophys. Res. Lett.*, **22**, 1973–1976.
- Bürgmann, R., Kogan, M.G., Levin, V.E., Scholz, C.H., King, R.W. & Steblow, G.M., 2001. Rapid aseismic moment release following the 5 December, 1997 Kronotsky, Kamchatka, earthquake, *Geophys. Res. Lett.*, **28**, 1331–1333.
- DeMets, C., Gordon, R.G., Argus, D.F. & Stein, S., 1994. Effect of recent revisions to the geomagnetic reversal time scale on estimates of current plate motions, *Geophys. Res. Lett.*, **21**, 2191–2194.
- Dziewonski, A.M., Ekstrom, G. & Maternovskaya, N.N., 1998. Centroid-moment tensor solutions for October–December 1997, *Phys. Earth planet. Inter.*, **109**, 93–105.
- Gusev, A.A. & Pavlov, V.M., 1998. Preliminary determination of parameters of the high-frequency source for the December 05, 1997, $M_w=7.9$ Kronotsky earthquake, *XXVI General Assembly, Eur. seism. Commission, Tel Aviv, Israel*, 73–77.
- Gusev, A., Levina, V., Saltykov, V. & Gordeev, E., 1998. Large Kronotsky earthquake of December 5, 1997: basic data, seismicity of the epicentral zone, source mechanism, macroseismic effects, in *Kronotskoe Earthquake of December 5, 1997 on Kamchatka: Precursors, Properties, Effects*, pp. 32–54, eds Gordeev, E.I., Ivanov, B.V. & Vikulin, A.V., Petropavlovsk, Kamchatsky.
- Klotz, J. *et al.*, 1999. GPS-derived deformation of the Central Andes including the 1995 Antofagasta $M_w=8.0$ earthquake, *Pure appl. Geophys.*, **154**, 709–730.
- Larson, K.M. & Lisowski, M., 1988. Strain accumulation in the Shumagin Islands: results of initial GPS measurements, *Geophys. Res. Lett.*, **21**, 489–492.
- Lisowski, M., Savage, J.C., Prescott, W.H. & Gross, W.K., 1988. Absence of strain accumulation in the Shumagin seismic gap, Alaska, 1980–1987, *J. geophys. Res.*, **93**, 7909–7922.
- Savage, J.C., Svarc, J.L. & Prescott, W.H., 1999. Deformation across the Alaska-Aleutian subduction zone near Kodiak, *Geophys. Res. Lett.*, **26**, 2117–2120.
- Takahashi, H. *et al.*, 1999. Velocity field around the Sea of Okhotsk and Sea of Japan region determined from new continuous GPS network data, *Geophys. Res. Lett.*, **26**, 2533–2536.
- Taylor, M.A.J., Zheng, G., Rice, J.R., Stuart, W.D. & Dmowska, R., 1996. Cyclic stressing and seismicity at strongly coupled subduction zones, *J. geophys. Res.*, **101**, 8363–8381.